Editors' Suggestion | Featured in Physics

Petawatt Laser Guiding and Electron Beam Acceleration to 8 GeV in a Laser-Heated Capillary Discharge Waveguide

A. J. Gonsalves,[1,*] K. Nakamura,[1] J. Daniels,[1] C. Benedetti,[1] C. Pieronek,[1,2] T. C. H. de Raadt,[1] S. Steinke,[1] J. H. Bin,[1] S. S. Bulanov,[1] J. van Tilborg,[1] C. G. R. Geddes,[1] C. B. Schroeder,[1,2] Cs. Tóth,[1] E. Esarey,[1] K. Swanson,[1,2] L. Fan-Chiang,[1,2] G. Bagdasarov,[3,4] N. Bobrova,[3,5] V. Gasilov,[3,4] G. Korn,[6] P. Sasorov,[3,6] and W. P. Leemans[1,2,†]

[1]*Lawrence Berkeley National Laboratory, Berkeley, California 94720, USA*
[2]*University of California, Berkeley, California 94720, USA*
[3]*Keldysh Institute of Applied Mathematics RAS, Moscow 125047, Russia*
[4]*National Research Nuclear University MEPhI (Moscow Engineering Physics Institute), Moscow 115409, Russia*
[5]*Faculty of Nuclear Science and Physical Engineering, CTU in Prague, Brehova 7, Prague 1, Czech Republic*
[6]*Institute of Physics ASCR, v.v.i. (FZU), ELI-Beamlines Project, 182 21 Prague, Czech Republic*

(Received 7 December 2018; revised manuscript received 30 January 2019; published 25 February 2019)

Guiding of relativistically intense laser pulses with peak power of 0.85 PW over 15 diffraction lengths was demonstrated by increasing the focusing strength of a capillary discharge waveguide using laser inverse bremsstrahlung heating. This allowed for the production of electron beams with quasimonoenergetic peaks up to 7.8 GeV, double the energy that was previously demonstrated. Charge was 5 pC at 7.8 GeV and up to 62 pC in 6 GeV peaks, and typical beam divergence was 0.2 mrad.

DOI: 10.1103/PhysRevLett.122.084801

Laser plasma accelerators (LPAs) [1,2] have large acceleration gradients of tens to hundreds of GV/m, which is several orders of magnitude larger than conventional radio frequency technology. This could allow for compact accelerators in a variety of applications, including free-electron lasers [3–5], Thomson sources [6,7], and electron-positron colliders with TeV energy [8,9]. For future efficient colliders using PW-class laser systems, single-stage energy gains of about 10 GeV are required [9]. Electron beams with energy up to a few GeV have been observed using nonpreformed plasmas and petawatt laser systems [10–12]. Preformed plasma waveguides can be used to mitigate laser diffraction of focused laser pulses, which increases the acceleration length and the energy gain for a given laser power. Using a capillary discharge waveguide to confine laser pulses over a distance of 9 cm, electron beams with energy up to 4.2 GeV were produced using a lower peak laser power of 300 TW [13].

The energy gain of a single-stage LPA [1] scales inversely with plasma density, n_0, since the accelerating gradient scales as $E_z \propto n_0^{1/2}$, and the length is limited to the laser-depletion length, which scales as $L_d \propto n_0^{-3/2}$. This scaling shows that in order to increase the energy gain to ≈ 10 GeV, the plasma density must be lowered relative to past experiments [10–13]. However, in order to accelerate over the full laser-depletion length and achieve maximum energy gain, diffraction of the focused laser pulses and the associated reduction in laser intensity must be mitigated. This laser pulse guiding can be achieved with a preformed plasma channel, in which the electron density is lower on axis, creating a refractive index profile that is peaked on axis [14], as is the case with graded-index optical fibers. For a parabolic channel with density rise (channel depth) Δn at a radius r_{ch} given by $n(r) = n_0 + (\Delta n / r_{\mathrm{ch}}^2) r^2$, a low intensity transversely Gaussian laser pulse can propagate with constant spot size when the input laser mode size equals the matched spot size of the channel ($r_0 = r_m$), where $r_m = [\pi r_e (\Delta n / r_{\mathrm{ch}}^2)]^{-1/4}$ and r_e is the classical electron radius. The capillary discharge waveguide [15] has been shown to be an effective method both of producing plasma channels and increasing energy gain in laser plasma accelerators through increased acceleration length [13,16,17]. The discharge current ionizes and heats the plasma via Ohmic heating. Since the plasma cools at the capillary wall, a temperature maximum and density minimum is formed on the capillary axis [18]. In order to increase energy gain toward 10 GeV [19], the laser power must be increased to the petawatt level, the plasma density reduced to $\approx 2 \times 10^{17}$ cm^{-3}, and the guiding achieved over twice the number of diffraction ranges ($\approx 15\ Z_R$) relative to previous experiments [13]. However, at this plasma density, and for the capillary diameter required to avoid laser damage, the capillary discharge waveguide produces a channel that is not deep enough to sufficiently confine the laser pulse.

In this Letter we show that the channel depth of a capillary discharge waveguide can be increased using laser pulses of nanosecond length to locally heat the plasma along the capillary axis [20], and that this structure can extend the LPA length to 20 cm (15 diffraction lengths) at low ($\approx 3.0 \times 10^{17}$ cm^{-3}) density. This enabled the generation of electron beams with quasimonoenergetic peaks in energy up to 7.8 GeV using a peak laser power of 850 TW.

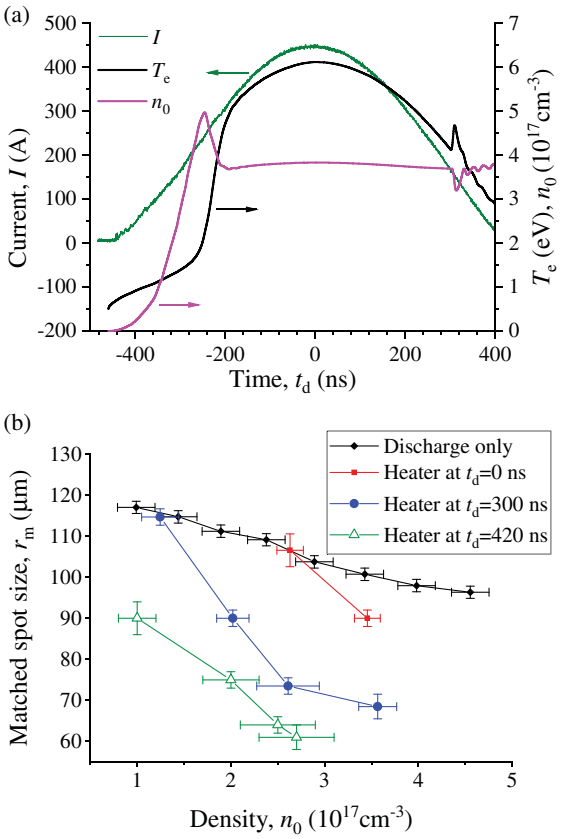

FIG. 1. (a) The measured discharge current temporal profile (green), along with the simulated on-axis temperature (black), and density (magenta). The heater pulse arrived at time 300 ns, causing the short-duration temperature rise and density reduction. (b) The matched spot size vs density for the 800 μm-diameter capillary with discharge alone (black), with the heater pulse arrival at the peak of discharge current (red squares), and with the heater pulse arrival 300 ns (blue circles) and 420 ns (green triangles) after the peak of the discharge current. The matched spot size is measured at the peak of the heater laser pulse and the error bars correspond to the standard deviation of the data.

A single high-energy laser plasma accelerator stage such as this, with future improvements in beam quality through controlled injection, could drive a hard x-ray FEL or serve as a building block of a high energy collider.

Laser heating [21,22] using a ns-duration matched pulse inside a capillary discharge waveguide to increase channel depth was proposed in Ref. [20]. In this concept, a "heater" laser pulse is guided by the discharge plasma and heats the plasma locally near the axis via inverse bremsstrahlung (IB) at rates on the order of 1 eV/ns. This creates a density depression through hydrodynamic motion, in addition to that created by the existing discharge-based channel. In the magneto-hydrodynamic (MHD) simulation of Ref. [20] a 1 ns-FWHM heater pulse was focused onto a capillary of diameter 1 mm. The 1D simulation did not take into account longitudinal laser evolution, but the laser focal spot size was chosen to be the matched spot size of the discharge channel to minimize longitudinal variation of the heater spot size, and, hence, plasma density. The heater pulse reduced the simulated matched spot size of the channel from 145 μm with the discharge alone to 100 μm, which is not sufficiently low to confine the wakefield "driver" laser pulses used in this experiment, which are focused to $r_0 \approx 60$ μm. One potential path to reducing the matched spot size further is to employ a smaller heater pulse focal spot size. However this would cause the heater pulse to be mismatched and give rise to oscillations in spot size and hence r_m, which can lead to reduced electron beam acceleration or loss of beam charge.

In the experiments and simulations presented here, a longer heater pulse that undergoes self-guiding is used so that it need not be constrained by the low power matching condition. Self-guiding in the case of a $\gtrsim$1 ns heater pulse occurs because the tail encounters a plasma that is already modified by IB heating and hydrodynamic motion. This can be understood from the ion acoustic speed, $c_s = (\gamma k T_e Z/m_i)^{1/2}$, where $\gamma \simeq 1.6$, k, Z, and m_i are the adiabatic index, Boltzmann constant, charge state, and ion mass, respectively. For the typical initial electron temperature T_e of the capillary discharge plasma (a few eV), $c_s \approx 20$ μm/ns, such that the tail of the heater pulse encounters a reduced on-axis density and lower matched spot size. This means that the requirement that the heater pulse focused spot size be equal to the low-power matched spot size of the initial plasma channel can be relaxed, allowing for a tighter focus of the heater pulse, and, hence, reduced r_m after heating. This effect is exploited here by using laser pulses of length 8 ns that undergo considerable self-guiding during the pulse rise-time. MHD simulations performed using the multidimensional code MARPLE (Magnetically Accelerated Radiative Plasma Explorer) [23], with additional modules from INF&RNO [24,25] to calculate the heater laser pulse propagation, showed that although the front of the heater pulse was mismatched to the plasma channel, later temporal slices of the pulse could be propagated with less than 10% change in spot size.

In addition to reducing the heater pulse spot size and increasing its duration, the matched spot size can be optimized by adjusting the delay between the current and heater pulses. Since Ohmic heating is approximately proportional to the square of the current, the plasma temperature reduces on the downward slope of the discharge current pulse. For the experiments the heater pulse intensity I_h was below 10^{12} W cm^{-2}, so the IB heating rate R_h was approximately proportional to $n_i I_h T_e^{-3/2}$, where n_i is the ion density [21,22]. Therefore, lowering the initial electron temperature by adjusting the timing of the discharge current pulse was an effective method for increasing the heating rate and reducing the matched spot size.

To measure the effect of IB heating, heater laser pulses of wavelength $\lambda_h = 532$ nm, energy 300 mJ, and FWHM duration 8 ns (generated by a Nd:YAG laser system), were

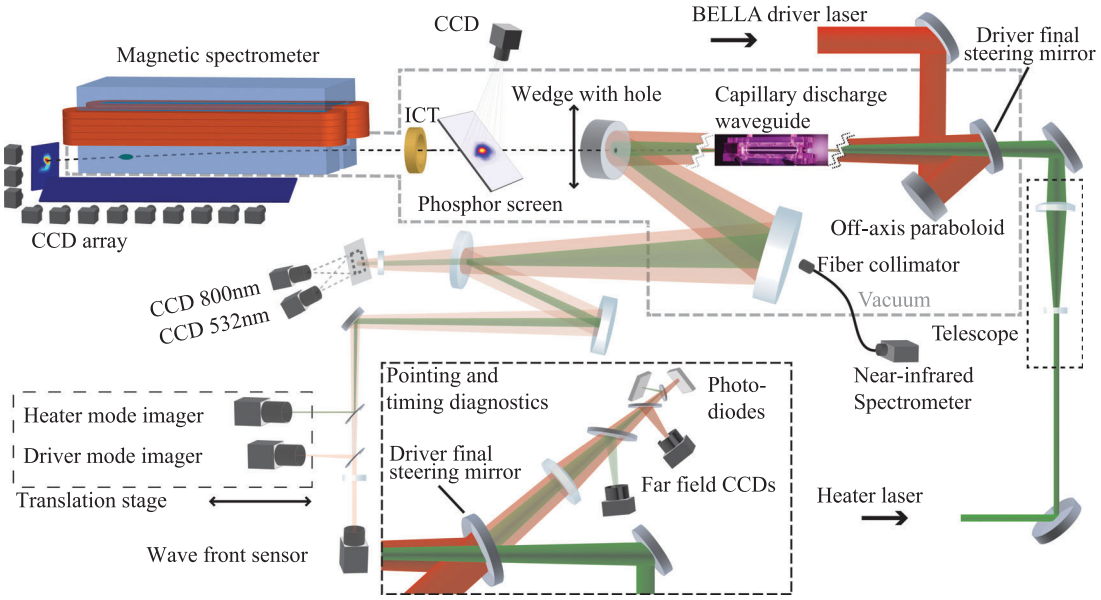

FIG. 2. Schematic layout of the BELLA LPA, including the heater laser system for enhancing the capillary discharge waveguide.

focused onto the capillary entrance to a spot size of $r_0 = 84\ \mu$m. Here r_0 is defined as the radius at which the intensity drops to $1/e^2$ of the peak value. Probe laser pulses with wavelength 800 nm and energy at nJ level were focused to a focal spot size $r_0 \approx 73\ \mu$m at the same location and arrived at the peak of the heater current pulse. The capillary discharge was operated with hydrogen using the current pulse shown in Fig. 1(a), which had an amplitude of 450 A and rise time of 400 ns. The capillary had a diameter of 800 μm and a length of 20 cm. Compared to Ref. [13], the capillary diameter was increased to mitigate damage from increased laser power, and the length increased to accelerate electrons to higher energy.

MARPLE simulations were performed using the experimentally measured current as input. The simulated temperature and on-axis plasma density are shown in Fig. 1(a). The temperature rises with the current through Ohmic heating. The density rises through ionization and drops through channel formation. After the peak of current the temperature drops due to reduced Ohmic heating and cooling at the capillary wall. The heater laser pulse arrived 300 ns after the peak of the discharge current, at which point the temperature rises from 4.1 to 4.7 eV, resulting in a reduction in on-axis density, indicating channel steepening and matched spot size reduction.

The matched spot size was measured by tracking centroid, spot size, and divergence oscillations of the probe pulse [26,27], and the density retrieved from measurements of the probe pulse group velocity in the plasma channel [28]. The relationship between the matched spot size and on-axis plasma density is shown in Fig. 1(b). The matched spot size without the heater (black line) was always significantly larger than the driver laser focal size of 60 μm, which results in poor guiding. For heater pulse arrival at the peak of current (red squares) as in Ref. [20], the matched spot size is reduced for a given density, consistent with IB heating. By timing the heater pulse to arrive $t_d = 300$ ns after the peak of the discharge current (blue circles), which reduces the plasma temperature and therefore increases the heating rate, the matched spot size reduction is even larger. For example at $n_0 = 3.4 \times 10^{17}$ cm^{-3}, the matched spot size was reduced from 101 μm to 69 μm. For $t_d = 420$ ns (green triangles), a matched spot size of 61 μm was generated with a density of 2.7×10^{17} cm^{-3}.

Note that for the high laser powers used for LPAs, laser guiding is achieved by a combination of channel guiding and self-guiding. Simulation of driver pulses with peak power 850 TW and $r_0 = 60\ \mu$m propagating through the laser-heated channel of matched spot size 69 μm were performed using the code INF&RNO. The laser intensity increased above the initially focused value due to the effects of self-focusing and self-steepening of the laser pulse. Efficient laser guiding was achieved, meaning that the laser intensity remained higher than the vacuum focal value until the last few cm of the capillary, at which point about half of the laser energy was depleted. This can be compared to a simulation for the same density without the heater, where a factor of 3.5 reduction in intensity was observed at only ≈ 6 cm into the capillary. Thus, for these parameters, self-guiding was not strong enough to compensate for the mismatched plasma channel. This poor guiding resulted in the loss of injected electrons as they entered a defocusing region of the wakefield (through the nonlinear decrease in plasma wavelength with decreasing intensity [1]), demonstrating the need for laser heating.

In the electron beam generation experiment, driver laser pulses at a wavelength of $\lambda = 815$ nm with spectral width 40 nm that were generated by the 1 Hz repetition rate

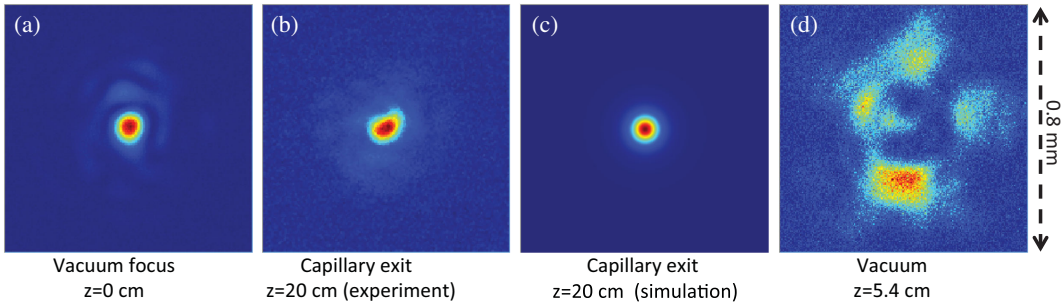

FIG. 3. Fluence profiles of 850 TW laser pulses: (a) measured at the entrance of the capillary (laser focal plane); (b) measured at the exit of the 20 cm-long capillary for $n_0 = 3.4 \times 10^{17}$ cm^{-3} and $r_m = 69$ μm; (c) retrieved from simulation at the same location as (b), and; (d) measured at 5.4 cm past the focal location with the capillary removed from the beam path. Each image has side equal to the capillary diameter of 0.8 mm. The measured results are from the driver mode imager (see Fig. 2).

Ti:sapphire-based BELLA petawatt laser [29] were focused to a focal spot size $r_0 \approx 60$ μm by a 13.5 m focal length off-axis parabolic mirror onto the entrance of a capillary waveguide as shown in Fig. 2. The laser energy at the focal location was 31 J, and the FWHM pulse duration was $\tau_0 \simeq 35$ fs as measured by a frequency resolved optical gating (FROG) system. The peak power was set to 850 TW, and the normalized laser strength was $a_0 = 8.5 \times 10^{-10} \lambda[\mu\text{m}] \sqrt{I_0[\text{W/cm}]^2} \simeq 2.2$ for the measured peak laser intensity I_0.

The laser beam diagnostics were described in Ref. [13], with the additions described below and shown in Fig. 2. Photodiodes were added to measure the delay between the driver and heater pulses, which was adjusted by changing the trigger time of the Nd:YAG laser. The root mean square (rms) fluctuation in delay was 0.3 ns. Heater beam cameras allowed for near and far field measurements to align the pulses and diagnose heater guiding. The first optical wedge after the waveguide was motorized so that for conditions where electron beams were not generated, the hole (which allows electrons to pass through to the electron beam diagnostics) could be translated out of the beam path to provide optimum imaging of the laser pulses.

The electron beam diagnostics were described in Ref. [13]. In this Letter, the phosphor screen images were used to measure the trajectory of the electron beam entering the magnetic spectrometer and increase the accuracy of the energy measurement. With the field that was applied to the magnetic spectrometer, the angular acceptance for the majority of the energy spectrum had a measurement range of $\approx \pm 0.5$ mrad. The milliradian shot-to-shot fluctuation in electron beam pointing meant that 10–20% of the electron beams fell within the acceptance of the magnetic spectrometer.

Figure 3 shows a focal spot at (a) the entrance with Strehl ratio 0.67 ± 0.05 and (b) the exit of the 20 cm-long capillary for laser power 850 TW in the spectral window 0.7–1 μm for $n_0 = 3.4 \times 10^{17}$ cm^{-3} and $r_m = 69$ μm, where the heater arrived $t_d = 300$ ns after the peak of the current pulse, and the driver arrived at the peak of the heater pulse. The exit mode size is approximately the same as input, which is consistent with the simulated result shown in Fig. 3(c). The simulation takes into account the limited spectral range of the diagnostic. To visualize the importance of guiding, the vacuum laser mode at 5.4 cm past focus is shown in Fig. 3(d), where $\approx 10\%$ of the laser energy resides outside the capillary radius. After 20 cm of propagation in vacuum (corresponding to the capillary exit plane), the laser diameter was approximately 2.4 mm.

For the conditions of Fig. 3(b), electron beams were observed on the phosphor screen and magnetic spectrometer. Examples of the electron beam spectra are shown in Fig. 4, where the entire measured spectrum is shown on the left of each row, and a 1.5 GeV-width subset of the highest energy peak from the same shot shown on the right. Due to the pointing fluctuations observed, the shots displayed are those in which the high energy component of the beam fell within the magnetic spectrometer acceptance. The total charge of the beams measured by the phosphor screen from (a) to (e) was 190, 320, 270, 210, and 420 pC. The charge in the spectral subsets was 24, 21, 40, 62, and 5 pC. For Fig. 4(e), where the highest energy peak of 7.8 GeV was observed, the discharge timing was adjusted so that the heater arrived 420 ns after the peak of the current pulse. At this delay and for the same density before heater pulse arrival, the initial plasma temperature was colder and the on-axis density and matched spot size were lowered to 2.7×10^{17} cm^{-3} and 61 μm, respectively.

Simulations of electron beam generation were performed with the code INF&RNO. The driver laser pulse input to the INF&RNO simulation had the measured parameters for the energy and temporal profile, and was approximated by a symmetrical jinc profile at focus as was done in Ref. [13]. For the parameters of Figs. 4(a)–(d), the density profile input to the INF&RNO simulation was obtained from a MARPLE simulation with input parameters close to the experiment. The heater laser pulse was approximated by a Gaussian with the experimentally measured value of $r_0 = 84$ μm. The simulated density profile had small longitudinal variations due to evolution of the heater pulse.

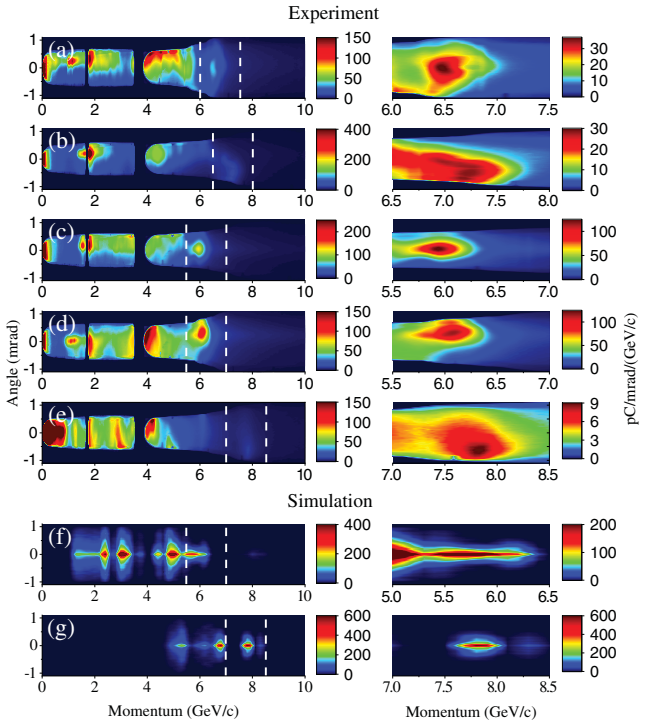

FIG. 4. (a)–(e): Electron beams measured by the magnetic spectrometer for $n_0 = 3.4 \times 10^{17}$ cm^{-3}, $r_m = 69$ μm and laser power 850 TW. The driver laser pulse arrival was timed with the peak of the heater pulse. The heater pulse arrived 300 ns after the peak of the discharge current, except for (e), where the delay was 420 ns, and the heater-induced density reduction was measured to be larger, with $n_0 = 2.7 \times 10^{17}$ cm^{-3} and $r_m = 61$ μm. The white dashed lines show the regions that are plotted in the right hand column, which shows the detailed spectrum of the highest energy peaks. The electron beam spectrum simulated by INF&RNO using the MARPLE-retrieved density profile (with $n_0 = 3.4 \times 10^{17}$ cm^{-3}) is shown in (f). In (g) a simulation is shown for the parameters of (e) using a transversely parabolic and longitudinally uniform density profile.

The minimum and maximum on-axis density values along the capillary were 3.35 and 3.41×10^{17} cm^{-3}, and the matched spot size varied between 68 and 72 μm. As in the experiment, the simulated spectrum shown in Fig. 4(f) shows multiple peaks in energy. In the simulation, electrons are first injected ≈ 5 cm into the capillary as a_0 rises above 3 due to self-steepening and self-guiding. Complex laser evolution at high power (including intensity and spectral changes), together with the effect of electron beam loading on the plasma, cause injection to start and stop several times as the pulse propagates through the plasma. This gives rise to several bunches of different final energy within the first plasma period, and a simulated charge of 430 pC. It should be noted that shot-to-shot fluctuations in the wave front of both lasers, as well as their relative pointing would change the plasma density profile and driver laser propagation. The divergence of the energy-integrated beams as measured on the phosphor screen was 0.2 ± 0.05 mrad FWHM and 0.6 ± 0.15 mrad rms, compared with the simulated results of 0.19 mrad FWHM and 0.35 mrad rms. The lower divergence from the simulation may be due to the assumption of cylindrical symmetry, since the measured laser mode (shown in Fig. 3) has nonsymmetric features.

Simulation of electron beam generation for $t_d = 420$ ns, presented in Fig. 4(g), showed a quasimonoenergetic peak at 7.8 GeV as observed in the experiment. The increase in beam energy was due to operation at lower density and reduced matched spot size, which allowed for effective guiding and acceleration over longer dephasing and pump depletion lengths. However, the simulation did not reproduce the significant charge at lower energy, perhaps related to the differences in the transverse plasma density profile or nonsymmetric spatial features of the laser pulse. It should be noted that in this nonlinear regime, trapping in multiple buckets and locations in the plasma often leads to charge in a broad energy range, but is sensitive to laser and plasma parameters.

In conclusion, IB heating inside a capillary discharge waveguide increased the channel depth and enabled the guiding of petawatt laser pulses at low density ($\approx 3 \times 10^{17}$ cm^{-3}) over ≈ 15 Z_R. The capillary discharge was used to guide the laser heater beam and to tune the laser heating rate and transverse density profile via control of the capillary fill pressure and discharge timing. The matched spot size of the channel was reduced from 106 μm to 61 μm via IB heating using self-guided heater laser pulses. For these conditions laser pulses with peak power up to 850 TW were guided over 20 cm, resulting in the generation of electron beams with hundreds of pC charge and multiple quasimonoenergetic peaks, the highest of which was at 7.8 GeV. This increase in energy compared to previous experiments using the same laser system [13] follows the expected energy gain scaling with density $\sim 1/n_0$ [1]. The energy gain and charge approach the designs required for future colliders and x-ray free-electron lasers. Further single-stage energy gain could be achieved at lower densities with approximately matched propagation using the BELLA PW laser system [19]. In addition to increasing energy gain, lowering the plasma density can mitigate dark current. In conjunction with controlled injection techniques [30–33], this can result in significantly reduced electron beam energy spread.

This work was supported by the Director, Office of Science, Office of High Energy Physics, of the U.S. Department of Energy under Contracts No. DE-AC02-05CH11231 and No. DE-FG02-12ER41798, the Alexander von Humboldt Foundation, NSF under Grant No. PHY-1632796, and Ministry of Education, Youth and Sports of Czech Republic under Grant No. CZ.02.2.69/0.0/0.0/16_027/0008465 and High Field Initiative (No. CZ.02.1.01/0.0/0.0/15_003/0000449), together with European Regional Development Fund. The simulations used the computational resources (Edison) of

the national energy research scientific computing center (NERSC). The authors gratefully acknowledge the technical support from Zac Eisentraut, Dave Evans, Mark Kirkpatrick, Art Magana, Greg Mannino, Joe Riley, Tyler Sipla, Austin Bajema, Will Waldron, Don Syversrud, and Nathan Ybarrolaza. The authors would also like to thank Eric Colby and Dieter Waltz for assistance with the magnetic spectrometer.

*ajgonsalves@lbl.gov
†wpleemans@lbl.gov

[1] E. Esarey, C. B. Schroeder, and W. P. Leemans, Rev. Mod. Phys. **81**, 1229 (2009).
[2] S. M. Hooker, Nat. Photonics **7**, 775 (2013).
[3] M. Fuchs, R. Weingartner, A. Popp, Z. Major, S. Becker, J. Osterhoff, I. Cortrie, B. Zeitler, R. Hörlein, G. D. Tsakiris, U. Schramm, T. P. Rowlands-Rees, S. M. Hooker, D. Habs, F. Krausz, S. Karsch, and F. Grüner, Nat. Phys. **5**, 826 (2009).
[4] Z. Huang, Y. Ding, and C. B. Schroeder, Phys. Rev. Lett. **109**, 204801 (2012).
[5] A. R. Maier, A. Meseck, S. Reiche, C. B. Schroeder, T. Seggebrock, and F. Grüner, Phys. Rev. X **2**, 031019 (2012).
[6] C. G. Geddes, S. Rykovanov, N. H. Matlis, S. Steinke, J. L. Vay, E. H. Esarey, B. Ludewigt, K. Nakamura, B. J. Quiter, C. B. Schroeder, Cs. Tóth, and W. P. Leemans, Nucl. Instrum. Methods Phys. Res., Sect. B **350**, 116 (2015).
[7] N. D. Powers, I. Ghebregziabher, G. Golovin, C. Liu, S. Chen, S. Banerjee, J. Zhang, and D. P. Umstadter, Nat. Photonics **8**, 28 (2014).
[8] W. Leemans and E. Esarey, Phys. Today **62**, No. 3, 44 (2009).
[9] C. B. Schroeder, E. Esarey, C. G. R. Geddes, C. Benedetti, and W. P. Leemans, Phys. Rev. ST Accel. Beams **13**, 101301 (2010).
[10] X. Wang *et al.*, Nat. Commun. **4**, 1988 (2013).
[11] H. T. Kim, K. H. Pae, H. J. Cha, I. J. Kim, T. J. Yu, J. H. Sung, S. K. Lee, T. M. Jeong, and J. Lee, Phys. Rev. Lett. **111**, 165002 (2013).
[12] H. T. Kim, V. B. Pathak, K. Hong Pae, A. Lifschitz, F. Sylla, J. H. Shin, C. Hojbota, S. K. Lee, J. H. Sung, H. W. Lee, E. Guillaume, C. Thaury, K. Nakajima, J. Vieira, L. O. Silva, V. Malka, and C. H. Nam, Sci. Rep. **7**, 10203 (2017).
[13] W. P. Leemans, A. J. Gonsalves, H. S. Mao, K. Nakamura, C. Benedetti, C. B. Schroeder, Cs. Tóth, J. Daniels, D. E. Mittelberger, S. S. Bulanov, J. L. Vay, C. G. R. Geddes, and E. Esarey, Phys. Rev. Lett. **113**, 245002 (2014).
[14] C. G. Durfee III and H. M. Milchberg, Phys. Rev. Lett. **71**, 2409 (1993).
[15] D. J. Spence and S. M. Hooker, Phys. Rev. E **63**, 015401 (2000).
[16] W. P. Leemans, B. Nagler, A. J. Gonsalves, Cs. Tóth, K. Nakamura, C. G. R. Geddes, E. Esarey, C. B. Schroeder, and S. M. Hooker, Nat. Phys. **2**, 696 (2006).
[17] T. P. A. Ibbotson *et al.*, Phys. Rev. ST Accel. Beams **13**, 031301 (2010).
[18] N. A. Bobrova, A. A. Esaulov, J.-I. I. Sakai, P. V. Sasorov, D. J. Spence, A. Butler, S. M. Hooker, and S. V. Bulanov, Phys. Rev. E **65**, 016407 (2001).
[19] C. Benedetti, C. B. Schroeder, T. Mehrling, B. Djordjevic, S. Bulanov, C. G. R. Geddes, E. Esarey, and W. P. Leemans, *Proceedings of 2018 IEEE Advanced Accelerator Concepts Workshop, Breckenridge, Colorado*, http://aac2018.org/, p. 43.
[20] N. A. Bobrova, P. V. Sasorov, C. Benedetti, S. S. Bulanov, C. G. R. Geddes, C. B. Schroeder, E. Esarey, and W. P. Leemans, Phys. Plasmas **20**, 020703 (2013).
[21] A. Y. Polishchuk and J. Meyer-Ter-Vehn, Phys. Rev. E **49**, 663 (1994).
[22] N. David, D. J. Spence, and S. M. Hooker, Phys. Rev. E **70**, 056411 (2004).
[23] V. Gasilov, A. Boldarev, S. Dyachenko, O. Olkhovskaya, E. Kartasheva, G. Bagdasarov, S. Boldyrev, I. Gasilova, V. Shmyrov, S. Tkachenko, J. Grunenwald, and T. Maillard, *Towards an Application of High-Performance Computer Systems to 3D Simulations of High Energy Density Plasmas in Z-Pinches*, Advances in Parallel Computing Vol. 22 (IOS Press, Amsterdam, Netherlands, 2012), pp. 235–242, DOI: 10.3233/978-1-61499-041-3-235.
[24] C. Benedetti, C. B. Schroeder, E. Esarey, C. G. R. Geddes, and W. P. Leemans, in *Proceedings of the 2010 Advanced Acceleration Concepts Work*, edited by G. Nusinovich and S. Gold (AIP, New York, 2010), Vol. 1299, pp. 250–255.
[25] C. Benedetti, C. B. Schroeder, C. G. Geddes, E. Esarey, and W. P. Leemans, Plasma Phys. Controlled Fusion **60**, 014002 (2018).
[26] A. J. Gonsalves, K. Nakamura, C. Lin, J. Osterhoff, S. Shiraishi, C. B. Schroeder, C. G. R. Geddes, Cs. Tóth, E. Esarey, and W. P. Leemans, Phys. Plasmas **17**, 056706 (2010).
[27] P. S. Antsiferov, M. R. Akdim, and H. T. Van Dam, Rev. Sci. Instrum. **78**, 123107 (2007).
[28] J. van Tilborg, J. Daniels, A. J. Gonsalves, C. B. Schroeder, E. Esarey, and W. P. Leemans, Phys. Rev. E **89**, 063103 (2014).
[29] K. Nakamura, H.-S. Mao, A. J. Gonsalves, H. Vincenti, D. E. Mittelberger, J. Daniels, A. Magana, Cs. Tóth, and W. P. Leemans, IEEE J. Quantum Electron. **53**, 1200121 (2017).
[30] B. B. Pollock, C. E. Clayton, J. E. Ralph, F. Albert, A. Davidson, L. Divol, C. Filip, S. H. Glenzer, K. Herpoldt, W. Lu, K. A. Marsh, J. Meinecke, W. B. Mori, A. Pak, T. C. Rensink, J. S. Ross, J. Shaw, G. R. Tynan, C. Joshi, and D. H. Froula, Phys. Rev. Lett. **107**, 045001 (2011).
[31] C. G. R. Geddes, K. Nakamura, G. R. Plateau, C. Toth, E. Cormier-Michel, E. Esarey, C. B. Schroeder, J. R. Cary, and W. P. Leemans, Phys. Rev. Lett. **100**, 215004 (2008).
[32] A. J. Gonsalves, K. Nakamura, C. Lin, D. Panasenko, S. Shiraishi, T. Sokollik, C. Benedetti, C. B. Schroeder, C. G. R. Geddes, J. van Tilborg, J. Osterhoff, E. Esarey, Cs. Tóth, and W. P. Leemans, Nat. Phys. **7**, 862 (2011).
[33] L. L. Yu, E. Esarey, C. B. Schroeder, J. L. Vay, C. Benedetti, C. G. R. Geddes, M. Chen, and W. P. Leemans, Phys. Rev. Lett. **112**, 125001 (2014).